Gain-scheduling control of dynamic lateral lane change for automated and connected vehicles based on the multipoint preview

Zhigen Nie, Zhongliang Li, Wanqiong Wang, Weiqiang Zhao, Yufeng Lian, Rachid Outbib

IET Intelligent Transport Systems

Research Article

IET Journals
The Institution of Engineering and Technology

Gain-scheduling control of dynamic lateral lane change for automated and connected vehicles based on the multipoint preview

ISSN 1751-956X
Received on 10th February 2020
Revised 29th May 2020
Accepted on 28th July 2020
E-First on 2nd September 2020
doi: 10.1049/iet-its.2020.0050
www.ietdl.org

Zhigen Nie[1,2], Zhongliang Li[2] ✉, Wanqiong Wang[1], Weiqiang Zhao[3], Yufeng Lian[4], Rachid Outbib[2]

[1]*Faculty of Transportation Engineering, Kunming University of Science and Technology, Kunming 650500, Yunnan, People's Republic of China*
[2]*LIS Lab (UMR CNRS 7020), Aix-Marseille University, 13397, Marseille, France*
[3]*State Key Laboratory of Automobile Dynamic Simulation, Jilin University, Changchun 130022, Jilin, People's Republic of China*
[4]*School of Electrical and Electronic Engineering, Changchun University of Technology, Changchun 130012, Jilin, People's Republic of China*
✉ *E-mail: zhongliang.li@lis-lab.fr*

Abstract: Dynamic lateral lane change (DLLC) control of automated and connected vehicles (ACVs) is challenging because of the time-varying and complex properties of the traffic environment. This study proposes a DLLC control strategy combining dynamic trajectory planning and tracking. According to the real-time longitudinal accelerations and velocities of multiple surrounding vehicles, as well as the real-time states of the ACVs, the safe trajectory reference of DLLC is obtained by solving a case-dependent constrained optimisation problem. The lane changing efficiency, vehicle stability and passenger comfort are considered jointly in the trajectory planning. Then, the dynamic trajectory reference is tracked through a gain-scheduling control algorithm combining previewed trajectory feed-forward and ACVs states feedback. Gain-scheduling control algorithm based on a linear time-varying form is utilised to achieve the precise control of the different velocities and improve the real-time ability of the algorithm. The proposed strategy is tested through software and hardware-in-loop experiments, and in different test scenarios. The results of simulations and experiments show that the proposed control strategy can achieve a satisfactory performance of DLLC. The lane changing efficiency, safety, passenger comfort and vehicle stability are verified in complex traffic environments.

Nomenclature

X_s, Y_s, Z_s	X-, Y-, Z-axes of vehicle coordinate system
δ_f	steering angle
F_{y1}	lateral force of the front axle
F_{y2}	lateral force of the rear axle
k_1	cornering stiffness of the front tire
k_2	cornering stiffness of the rear tire
I_{zz}	moment of inertia around Z-axis
I_{xz}	yaw roll product of inertia
I_{xeq}	moment of inertia around X-axis
a	distance from the centre of mass to the front axle
b	distance from the centre of mass to the rear axle
u_m	vehicle velocity
u_{sx}, u_{sy}	longitudinal and lateral velocity in the vehicle coordinate system
$\beta, \dot{\beta}$	sideslip angle and angle velocity
$\psi, \dot{\psi}, \ddot{\psi}$	yaw angle, angle velocity and angle acceleration
$\phi, \dot{\phi}, \ddot{\phi}$	yaw angle, angle velocity and angle acceleration
k_s	roll stiffness
c_s	roll damping
m, m_s	mass and sprung mass
h	distance from the centroid of mass to roll axis
h	distance from the centroid of mass to roll axis
ΔM	distance from the centroid of mass to roll axis
K	control gain
$Y_{r1} \ldots Y_{rn}$	desired lateral displacement
ψ_d	desired lateral displacement
δ	angle of the steering wheel
p_{ij}	the pressure of four cylinder
t	time
T	sample time
X_r, Y_r	longitudinal and lateral displacement
Re	lane width
D	longitudinal length of the trajectory
D_{lf}	maximum limit determined by the front vehicle of the target lane (C vehicle)
D_{lr}	maximum limit determined by the rear vehicle of the target lane (B vehicle)
D_{zf}	maximum limit determined by the front vehicle of the original lane (E vehicle)
$65\ \mathrm{km\ h^{-1}}$	maximum limit determined by the rear vehicle of the original lane (D vehicle)
u_{gx}, u_{gy}	longitudinal and lateral velocity in the global coordinate system
u_{sx}, u_{sy}	longitudinal and lateral velocity in the vehicle coordinate system
D_{lf0}	initial distance between ACVs and C vehicle
D_{lf1}	ACV driving distance from the start to the real-time position under the situation of C vehicle
D_{lf2}	driving distance of C vehicle from the start to real-time position
D_{lf3}	predicted driving distance of C vehicle from real-time to the predicted position
D_{lf4}	predicted position under the situation of C vehicle
u_{lf0}	initial velocity of C vehicle
a_{lf}	initial acceleration of C vehicle
u_{lfr}	velocity acceleration of C vehicle at the real-time
t_{lf}	time from the real-time to the predicted time when ACV lateral lane change will be completed
a_{lfr}	longitudinal acceleration of C vehicle at the real-time
$a_{x,\max}$	maximum longitudinal deceleration
l_{sa}	distance from the front end to the centroid position of the ACVs
l_{lfb}	distance from the rear end to the centroid position of C vehicle
D_{zf0}	initial distance between ACVs and E vehicle
D_{zf1}	real-time position under the situation of E vehicle
D_{zf2}	driving distance of E vehicle from the start to the real-time position

D_{zf3}	predicted driving distance of E vehicle from real-time to the predicted position
D_{zf4}	ACV driving distance from real-time to the predicted position under the situation of E vehicle
u_{zf0}	initial acceleration of E vehicle
a_{zf}	longitudinal acceleration of E vehicle
μ_1, μ_2	angles shown in Fig. 5*c*
l_{sw}	ACVs width
l_{zfa}	longitudinal distance from right-front position to the *Y*-axis of ACVs
Δl_{zfb}	longitudinal distance from limit position to centroid position of E vehicle
X_{zf}, Y_{zf}	longitudinal and lateral displacement at the predicted limit position of obstacle avoidance
l_{zfw}	E vehicle width
l_{zrw}	D vehicle width
$a_{y,\max}$	maximum lateral acceleration of trajectory
$a_{y,s,\max}$	maximum safe lateral acceleration of trajectory
t_c	completed time of lateral lane change
$t_{\max}$	maximum allowed cost time of lateral lane change
η	weight factor
$\dot{Y}_r$, $\ddot{Y}_r$	first and second derivatives of the trajectory function equation
X, Y	real-time longitudinal and lateral displacement of ACVs
t_p	time from start to real-time
$u_{\min}$, $u_{\max}$	maximum and minimum of ACV longitudinal velocity
e_y	error of lateral displacement
e_ψ	error of yaw angle
a_y	lateral acceleration of ACVs
q_1	weight coefficient of lateral displacement error
q_2	weight coefficient of yaw angle error
q_3	weight coefficient of lateral acceleration
r_1	weight coefficient of steering angle
r_2	weight coefficient of additional torque
Y_s	lateral displacement in the vehicle coordinate system

1 Introduction

Traffic jams, vehicle safety problems have become more and more prominent. In 2016, traffic accidents led to 63,093 deaths, 226,430 injuries and directly 1.21 billion CNY of property losses in China [1]. According to the World Health Organization report, 93% of traffic accidents were caused by human error operation [2]. Developing automated and connected vehicles (ACVs) has been considered as an effective solution to reduce vehicle accidents. Besides, recent studies have demonstrated that the ACVs could lead up to 20% energy saving [3]. The lateral lane change of ACVs not only involves the control of the ACVs but also pays influence to the whole traffic. Improper lane change may result in collisions and vehicle instability and affects passenger comfort [4–6]. The ACS lateral lane change control is also considered as an important research issue [7–9].

The dynamic lateral lane change (DLLC) control consists of trajectory planning and trajectory tracking [10, 11]. The task of the trajectory planning is to obtain the optimal reference trajectory according to the dynamic environment and vehicle states; whereas the task of trajectory tracking is to track the trajectory reference precisely. The criteria, such as vehicle safety, vehicle stability and passenger comfort, are usually considered in the control design.

Increasing attention has been paid to trajectory planning. In [8, 12], the desired trajectory reference is obtained by optimising the parameters of a polynomial trajectory model to avoid stationary obstacles and fixed-speed obstacles. As lateral lane change seriously affects safety and traffic operation efficiency, some lane change planning algorithms seek to find the minimum lane-changing safety distance (see [13] for instance). Similarly, the trajectory is planned by assessing the risk level in [14]. Recently, the machine learning tools, such as fuzzy neural networks, have been increasingly evoked for trajectory planning purposes [15]. However, the above-mentioned studies assume that the speeds of surrounding vehicles (SVs) are constant, which could not be true in practice.

Some dynamic trajectory planning algorithms were proposed to plan the trajectory of lateral lane change considering the real-time states of SVs [16–18]. However, only one or two vehicles around the ACV are considered in these studies. In the actual traffic environment, more complex surrounding conditions can be encountered. Trajectory planning should be conducted under more complex and practical constraints.

As for trajectory tracking, Shah *et al.* [19] proposed a control strategy of rear anti-collision for lateral lane change using the electronic power steering system. Yu *et al.* [20] proposed a control strategy of trajectory tracking using a specially designed hierarchical controller. To improve vehicle stability, some control algorithms were presented and tested in a high-speed trajectory tracking case [21–23]. Most control strategies in the above studies are designed to track the instantaneous trajectory reference of vehicle lateral displacement or yaw angle. In this framework, a multipoint preview is feed-forwarded to the control strategy to achieve good trajectory tracking performance with smaller fluctuation and control consumption [24, 25].

Robust control algorithms are receiving increasing attention for DLLC [26–29]. The results in the above studies reveal that robust control strategies can resist parameter uncertainties and external disturbances to achieve good trajectory tracking. However, these proposed robust control strategies involve only steering system control, which cannot sufficiently guarantee the safety of lateral lane change, especially in the emergency conditions.

Some control strategies combining a steering system with a braking system were proposed for trajectory tracking. In [30], an improved Hamilton algorithm was proposed to achieve obstacle avoidance. A model predictive control algorithm was studied for the same purpose in [12]. However, the ACV velocity change during lateral lane change is not considered in these studies. The control performance on tracking precision and robustness could be unsatisfactory regarding that the velocity of ACV is usually varied in the lane change process.

To overcome the shortcomings of the previous research, a DLLC control strategy is proposed in this work to improve the performance of both trajectory planning and tracking modules. In the control strategy, the studied traffic environment consists of controlled ACV and four SVs. The velocities and accelerations of the four SVs are time-varying. The considered traffic environment is close to an actual traffic environment. According to the dynamics of the SVs and the states of the ACV, the real-time limits of the trajectory are determined by respecting safe distances between the controlled ACV and the SVs. The real-time optimal trajectory reference is then found by coordinating lane change efficiency, vehicle stability and passenger comfort within the limits.

For trajectory tracking, the control algorithm is constructed by combining previewed trajectory feed-forward and ACVs states feedback. Gain-scheduling control algorithm based on a linear time-varying (LPV) form is utilised to achieve the precise control of different ACV velocities and improve the real-time ability. The control algorithm integrating steering and braking control is implemented to ensure the lane change safety under the emergency condition.

The main contributions of this paper are as follows:

(i) The real-time trajectory planning is realised in a more complex traffic environment which is close to reality. In particular, the possible non-smooth aspect of the trajectory tracked and the speed variability is taken into account.
(ii) The multiple trajectory points preview can be beneficial to cope with real-time dynamic trajectory tracking. Meanwhile, the gain-scheduling control algorithm based on the LPV form can deal with the time-varying ACV velocity and improve the real-time ability of the algorithm.
(iii) To overcome the shortcoming that the strategy with only the steering system cannot guarantee the stability of DLLC in emergency conditions, the proposed control strategy combines a

steering system with the braking system to maintain yaw and roll stability of the ACVs.

The remainder of this paper is structured as follows. Section 2 introduces the vehicle model dedicated to the design of the control strategy. The DLLC control strategy for the ACVs, including trajectory planning and tracking, is presented in Section 3. In Section 4, the simulations and HIL experiments are conducted in different scenarios. The results are analysed and discussed in the section. Finally, conclusions are made in Section 5.

2 Simplified vehicle model

The DLLC is determined by lateral motion and handing angle [28, 31]. Meanwhile, passenger comfort and vehicle stability are affected by the rolling motion during the lane change process. As shown in Fig. 1, three degrees of freedom (DOF) lateral vehicle model is established for control purpose [32].

The model involves three Kinematic equations of three freedoms, i.e. lateral, yaw and roll motions. The vehicle horizontal motion of ACVs is shown in the left figure, which mainly involves lateral displacement and heading angle and can represent vehicle yaw stability. In addition, the vertical roll motion of ACVs displays in the right figure, which can represent the vehicle roll stability. Therefore, the 3DOF model can be utilised to lateral displacement and heading angle tracking while improving ACVs yaw and roll stability. The model is represented as the following equations

$$mu_{sx}\left(\dot{\beta}+\dot{\psi}\right)-m_s h\ddot{\phi}=F_{y1}\cos\delta_f+F_{y2} \tag{1}$$

$$I_{zz}\ddot{\psi}-I_{xz}\ddot{\phi}=F_{y1}a\cos\delta_f-F_{y2}b+\Delta M \tag{2}$$

$$\begin{aligned} I_{x\mathrm{eq}}\ddot{\phi}-I_{xz}\ddot{\phi}=&\,m_s g h\phi+m_s h u_{sx}\left(\dot{\beta}+\dot{\psi}\right)\\ &\times\cos(\phi)-k_s\phi-c_s\dot{\phi}\end{aligned} \tag{3}$$

where the lateral forces of front and rear axles F_{y1} and F_{y2} can be expressed using the following tire model

$$F_{y1}=k_1\left(\beta+\frac{a}{u_{sx}}\dot{\psi}-\delta_f\right) \tag{4}$$

$$F_{y2}=k_2\left(\beta-\frac{b}{u_{sx}}\dot{\psi}\right) \tag{5}$$

The detailed assumptions and the description of the simplified vehicle model can be found in [33].

3 DLLC control strategy

To achieve good lateral lane change control performance for ACVs in complex traffic environments, a control strategy combing real-time optimisation based trajectory planning and enhanced LPV-based gain-scheduling tracking control is proposed.

As shown in Fig. 2, three steps are carried out in the modules of dynamic trajectory planning. (i) Four maximum longitudinal limits of safe lateral lane change trajectory for the ACV are calculated according to the states and positions of the ACV and SVs. (ii) According to the relative position of the ACV with respect to the SVs, the four maximum longitudinal limits are conditionally activated. (iii) The real-time trajectory reference of lateral lane change is obtained by optimising the designed objective function, within the real-time longitudinal limits. In the trajectory tracking module, the real-time desired lateral displacement and yaw angle are obtained through previewing the real-time optimal trajectory. The control algorithm is designed based on an LPV model to deal with the velocity change of the ACV. The feed-forward of trajectory preview is combined with the feedback of real-time states in the control design. The linear quadratic regulator (LQR) classical optimal control algorithm is used to configure the gain-scheduled controller. The steering angle and additional moment determined by the controller are transformed into the corresponding steering wheel angle and wheel cylinder pressure through a corresponding inverse model. Finally, the steering wheel angle and wheel cylinder pressure are applied to the virtual vehicle to achieve the ACV lateral lane change.

In the sequel, the detailed designs of the trajectory planning and tracking modules are described.

3.1 Dynamic trajectory planning of lateral lane change

The task of dynamic trajectory planning is to obtain the real-time optimal trajectory for lateral lane change of the ACV under complex traffic environment according to the dynamic change of the external environment and the states of the ACV. The module of dynamic trajectory planning is shown in Fig. 3 in detail. As shown in the flowchart, the modular of dynamic trajectory planning is divided into three sub-modules, namely the maximum longitudinal limits calculation, the decision of real-time limits and the real-time trajectory optimisation.

As shown in Fig. 4, the complex traffic system is composed of the ACV and other four SVs to represent the actual traffic environment. The trajectory of lateral lane change for the ACV is constrained by the four SVs. For each SV, the maximum safe longitudinal limit of the lateral lane changing trajectory is determined to guarantee that the ACV does not collide with the SV. As lateral lane change of the ACV proceeds, the real-time limit of lane changing trajectory is dynamically determined by synthesising the four maximum safe longitudinal limits. Finally, the real-time optimal lane change trajectory is obtained by maximising the lane change efficiency, the passenger comfort and the stability of the ACV within the real-time limit. In Fig. 4, the vehicles with the black solid line are the vehicles at the start time of the lateral lane change. The vehicles with the green solid line are the real-time vehicles and the vehicles with the purple dashed line are the vehicles of the predicted time when lateral lane change will be

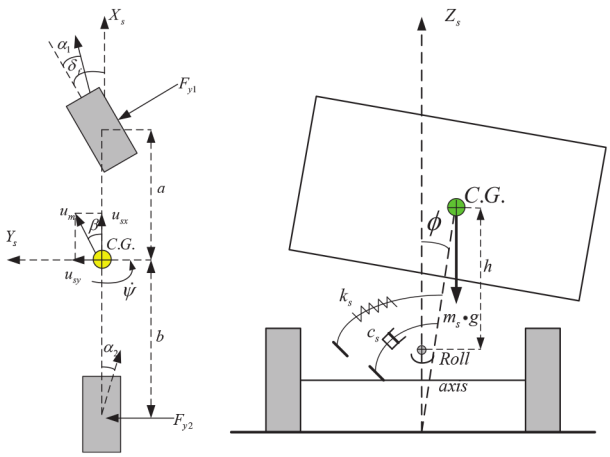

Fig. 1 *Sketch map of 3-DOF simplified model*

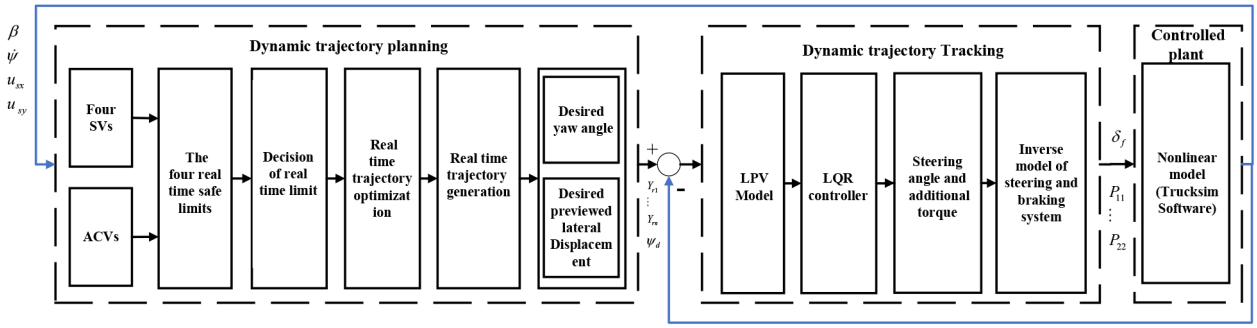

Fig. 2 *Sketch map of control strategy*

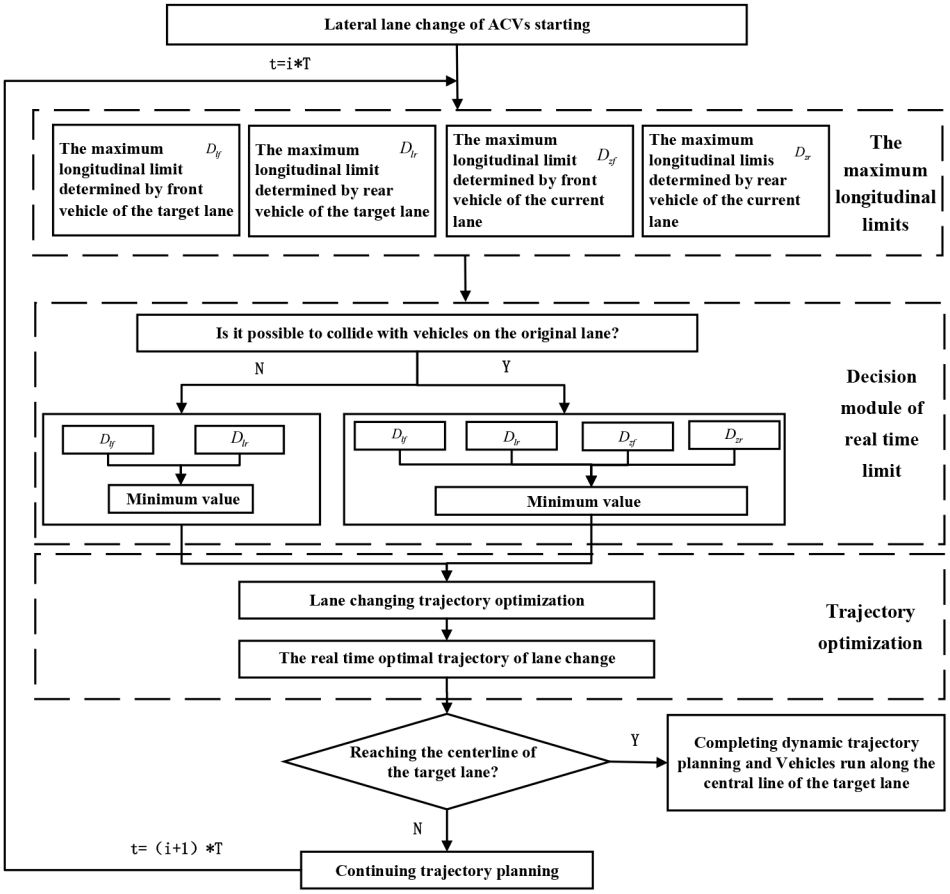

Fig. 3 *Flow chart of real time optimal trajectory planning for lateral lane change*

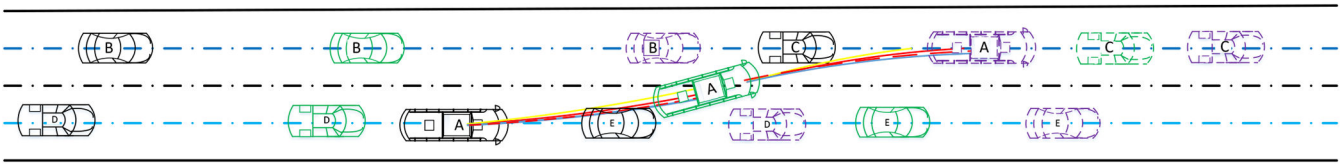

Fig. 4 *Complex traffic environment of typical lateral lane change for ACVs (the vehicles with the black solid line are the vehicles at the start time, the vehicles with the green solid line are the real-time vehicles, the vehicles with purple dashed line are the vehicles at the predicted time when lateral lane change will be completed, the yellow solid lines, red dotted lines and red dotted lines are the trajectories met the maximum limit, the blue solid lines is the real time maximum limit, the red solid line is the real time optimal trajectory)*

completed. There are yellow solid lines, red dotted lines and red dotted lines which all meet the maximum limit. The real-time maximum limit is the blue solid lines. Through the optimisation algorithm, the red solid line is obtained as a real-time optimal trajectory of the lateral lane change.

3.1.1 Longitudinal limits of the trajectory: To simply and efficiently generate the dynamic trajectory of lateral lane change and ensure the lateral velocity to zero when the ACVs enter target lane, the cosine curve is used as the basic curve for the dynamic trajectory planning of lateral lane change. The curve function is as follows [5, 13]:

$$Y_{\mathrm{r}} = \frac{\mathrm{Re} * X_{\mathrm{r}}}{D} - \frac{\mathrm{Re}}{2\pi} * \sin\left(\frac{2\pi X_{\mathrm{r}}}{D}\right) \tag{6}$$

As the lane width is usually fixed, the curve shape is determined by the longitudinal length D of the curve. According to the real-time information of the ACV and SVs, such as the velocity, acceleration etc. the real-time trajectory of lateral lane change can be

dynamically adjusted by changing the planned longitudinal length D.

As shown in Fig. 4, the controlled ACV and the four SVs are used to represent the practical complex traffic environment. The planned trajectory should guarantee safe distances from the four SVs. Hence, four constraints are established as follows:

Maximum longitudinal limit determined by the vehicles on the target lane: The location relationship of the ACVs and the front vehicle on the target lane (C vehicle) is shown in Fig. 4. The vehicles with the black solid line are the vehicles at the start time of the lateral lane change. The vehicles with the green solid line are the real-time vehicles and the vehicles with the purple dashed line are the vehicles of the predicted time when the lateral lane change is completed. The yellow dotted line trajectory is the trajectory planned before the current moment. The red solid line trajectory is the maximum longitudinal limit planned in real-time.

The velocity of the ACV can be transformed from the vehicle coordinate system to the global coordinate system, as

$$u_{gx} = u_{sx}\cos\psi - u_{sy}\sin\psi \tag{7}$$

$$u_{gy} = u_{sx}\sin\psi + u_{sy}\cos\psi \tag{8}$$

The longitudinal driving distance of the ACV from the start position to real-time position

$$D_{lf1} = \int_{gx}^{u} \mathrm{d}t \tag{9}$$

The longitudinal driving distance of C vehicle from the start position to real-time position

$$D_{lf2} = \int^{(} u_{lf0} + a_{lf}t)\,\mathrm{d}t \tag{10}$$

The predicted driving longitudinal distance of C vehicle from real-time position to the predicted position where lateral lane change will be completed can be real-time obtained through assuming that longitudinal acceleration of C vehicle is constant from real-time position to the predicted position

$$D_{lf3} = u_{lfr}t_{lf} + \frac{1}{2}a_{lfr}(t_{lf})^2 \tag{11}$$

The longitudinal driving distance of the ACV from real-time position to the predicted position completed lateral lane change D_{lf4} can be obtained through assuming that the longitudinal velocity of the ACV is constant from real-time position to the predicted position

$$D_{lf4} = u_{gx}t_{lf} \tag{12}$$

The velocity of C vehicle at the predicted position where the lateral lane change u_{lfc} will be completed is given by

$$u_{lfc} = u_{lfr} + a_{lfr}t_{lf} \tag{13}$$

It is necessary to leave a certain distance to avoid a collision when the lane changing is completed. The minimum distance is obtained by decelerating the two vehicles with the maximum deceleration as follows:

$$l_{lf} = \frac{(u_{gx})^2}{2a_{x\max}} - \frac{(u_{lfc})^2}{2a_{x\max}} \tag{14}$$

The maximum limit is reached as the following geometric relation holds:

$$D_{lf2} + D_{lf3} = D_{lf1} + D_{lf4} + l_{sa} + l_{lf} + l_{lfb} - D_{lf0} \tag{15}$$

The predicted time t_{lf} can be obtained from (15). D_{lf4} can be obtained based on (12) using t_{lf}. Then, the maximum longitudinal limits determined by C vehicle D_{lf} can be obtained, as

$$D_{lf} = D_{lf1} + D_{lf4} \tag{16}$$

Remark 1: as shown in Fig. 5*b*, the maximum of D relating to the rear vehicle on the targeted lane, i.e. D_{lr}, can be calculated similarly.

Maximum longitudinal limit determined by the vehicles on the original lane: The right front point of the ACV is prone to collide with the front vehicle on the original lane (vehicle E) in the process of the lateral lane change. Therefore, the maximum longitudinal limit determined by E vehicle is obtained based on the limit position of obstacle avoidance determined by the ACV and vehicle E (see Fig. 5*c*).

The longitudinal driving distance of the ACV from the start position to real-time position is

$$D_{zf1} = \int_{gx}^{u} \mathrm{d}t \tag{17}$$

The longitudinal driving distance of E vehicle from the start position to real-time position is

$$D_{zf2} = \int (u_{zf0} + a_{zf}t)\,\mathrm{d}t \tag{18}$$

Assuming that the longitudinal velocity and yaw angle of the ACV are constant, the longitudinal driving distance of the ACV from real-time position to predicted limit position of obstacle avoidance is calculated as

$$D_{zf3} = u_{gx}t_{zf} \tag{19}$$

Assuming that the longitudinal acceleration of E vehicle is constant, the longitudinal driving distance of E vehicle from real-time position to a predicted limit position of obstacle avoidance is

$$D_{zf4} = u_{zfr}t_{zf} + \frac{1}{2}a_{zf}(t_{zf})^2 \tag{20}$$

As shown in Fig. 5*c*, the angle formed by the right front point and centroid of the ACV at the limit position is

$$\mu_1 = a\tan\left(\frac{l_{sw}/2}{l_{zfa}}\right) \tag{21}$$

The lateral distance between the ACVs and edge of E vehicle is

$$h_{zf} = \sqrt{(l_{sw}/2)^2 + l_{zfa}^2}\sin(\psi - \mu) \tag{22}$$

The longitudinal difference between the centroid of the ACV and the centroid of E vehicle at the limit position is calculated as

$$\Delta l_{zf} = \Delta l_{fa} + \Delta l_{zfb} = \sqrt{(l_{sw}/2)^2 + l_{zfa}^2}\cos(\psi - \mu_1) + \Delta l_{zfb} \tag{23}$$

The limit of D is encountered as the following geometric relationship holds:

$$D_{zf0} + D_{zf2} + D_{zf4} = D_{zf1} + D_{zf3} + \Delta l_{zf} \tag{24}$$

The predicted time t_{zf} from real-time position to the predicted limit position of obstacle avoidance can be obtained using (24). D_{zf3} can then be obtained based on (19).

Longitudinal and lateral displacements at the predicted limit position of obstacle avoidance are calculated respectively, as

$$X_{zf} = D_{zf1} + D_{zf3} \tag{25}$$

$$Y_{zf} = \frac{l_{zfw}}{2} - h_{zf} \tag{26}$$

The maximum longitudinal limit determined by E vehicle is obtained by substituting (25), (26) into (6).

Remark 2: As shown in Fig. 5*d*, the maximum value of D relating to the rear vehicle on the original lane, i.e. D_{zr}, can be calculated similarly.

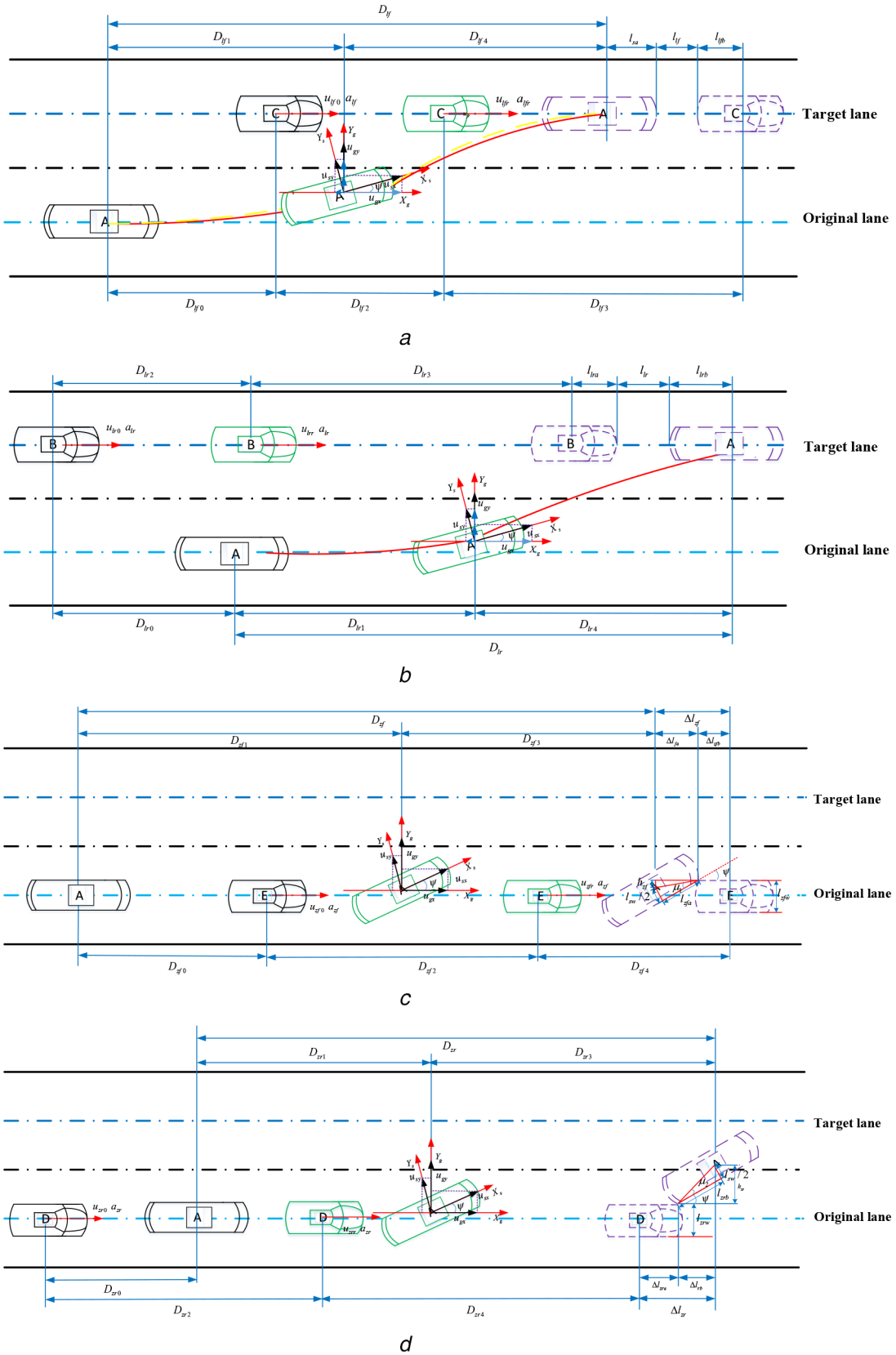

Fig. 5 *Maximum longitudinal length limit of lane change trajectory determined by four SVs*

(a) Determined by the front vehicle on the target lane, ***(b)*** Determined by the rear vehicle on the target lane, ***(c)*** Determined by the front vehicle on the original lane, ***(d)*** Determined by the rear vehicle on the original lane

3.1.2 Decision module of trajectory limit: Once the four maximum longitudinal limits are determined, it is necessary for the real-time to decide which limits should be considered in the trajectory planning. From Figs. 5*c* and *d*, it is seen that the ACV and the vehicles on the original lane do not collide when the lateral position of right rear points exceeds the outermost point of the vehicles on the original lane. The maximum longitudinal limits determined by the vehicles on the original lane should not be considered to plan the trajectory of ACVs after this case. In this case, the trajectory can be planned in a more slack condition. The judging criterion is formulated as

$$\begin{aligned} Y_{\mathrm{r}} &\geq \left(l_{z\mathrm{rw}}/2 - \sqrt{(l_{\mathrm{sw}}/2)^2 + l_{z\mathrm{fa}}^2}\sin(\psi - \mu_1)\right) \\ \text{and } Y_{\mathrm{r}} &\geq \left(\sqrt{(l_{\mathrm{sw}}/2)^2 + l_{z\mathrm{rb}}^2}\sin(\psi + \mu_2) + l_{z\mathrm{fw}}/2\right) \end{aligned} \tag{27}$$

If vehicle states satisfy (27), the real-time longitudinal limit is only determined by maximum longitudinal limits related to the vehicles on the target lane, as

$$D_{\max} = \mathrm{Min}(D_{\mathrm{lf}}, D_{\mathrm{lr}}) \tag{28}$$

If vehicle states do not satisfy (27), the real-time longitudinal limit is determined by the maximum longitudinal limits corresponding to the four vehicles on both the original and the target lane

$$D_{\max} = \mathrm{Min}(D_{\mathrm{lf}}, D_{\mathrm{lr}}, D_{z\mathrm{f}}, D_{z\mathrm{r}}) \tag{29}$$

3.1.3 Optimal trajectory of lane change: The objective functions of trajectory planning are designed considering the efficiency of the lane change, passenger comfort and roll stability, and is optimised within the real-time longitudinal limits. Thus, safety is also taken into account in trajectory planning.

The efficiency of lane changing can be characterised by the time of the lane change process. Whereas, passenger comfort and roll stability can be quantified by the lateral acceleration. However, efficiency is mutually contradictory with respect to comfort and roll stability. Therefore, the optimisation objective function is designed by balancing the two contradictory factors [16], as

$$Q = \eta\frac{|a_{y,\max}|}{|a_{y,\mathrm{s},\max}|} + (1-\eta)\frac{t_{\mathrm{c}}}{t_{\max}}, \quad 0 \leq \eta \leq 1 \tag{30}$$

The weights of the two factors can be adjusted by configuring η The lateral acceleration of the trajectory is formulated as

$$a_y = \rho * \left(u_{\mathrm{g}x}\right)^2 \tag{31}$$

where the curvature of the trajectory for lateral lane change is

$$\rho = \left|\frac{\ddot{Y}_{\mathrm{r}}}{\left(1 + \left(\dot{Y}_{\mathrm{r}}\right)^2\right)^{3/2}}\right| \tag{32}$$

According to (6), $\dot{Y}_{\mathrm{r}}$ and $\ddot{Y}_{\mathrm{r}}$ are deduced, respectively, as

$$\dot{Y}_{\mathrm{r}} = \frac{\mathrm{Re}}{D} - \frac{\mathrm{Re}}{D}\cos\left(\frac{2\pi X_{\mathrm{r}}}{D}\right) \tag{33}$$

$$\ddot{Y}_{\mathrm{r}} = \frac{2\pi\mathrm{Re}}{D^2}\sin\left(\frac{2\pi X_{\mathrm{r}}}{D}\right) \tag{34}$$

It is assumed that the real-time velocity $u_{\mathrm{g}x}$ is constant after the current time. The cost of time for lateral lane change is

$$t_{\mathrm{c}} = t_{\mathrm{p}} + \frac{D - X_{\mathrm{r}}}{u_{\mathrm{g}x}} \tag{35}$$

The optimal longitudinal length of lane change trajectory is obtained by minimising the objective function defined in (30) within the previously acquired constraints. The optimal real-time trajectory of lateral lane change can further be obtained using (6).

3.2 Tracking control of dynamic trajectory

To achieve the good effect of lateral lane change for ACVs, the dynamic planned trajectory must be accurately tracked using low control consumption and maintaining stable vehicle states. In [24, 25], the reference trajectory is fed to the controller through the multipoint preview operation. The control strategy is then designed by combining trajectory feed-forward with states feedback to obtain good effects of the reference trajectory tracking. The multipoint preview operation realises the human-like trajectory tracking control with the comfort easily accepted by passengers. Meanwhile, it is also demonstrated that low control consumption and stable vehicle states can be achieved with this control strategy [34].

3.2.1 State equation: The state equation dedicated to DLLC design is composed of the simplified vehicle model introduced in Section 2 and two additional equations relating to lateral displacement and yaw angle

$$\dot{x} = \boldsymbol{A}x + \boldsymbol{B}u \tag{36}$$

where

$$\begin{aligned} u &= [\delta_{\mathrm{f}}\ \Delta M]^{\mathrm{T}} \\ x &= \begin{bmatrix}\beta & \dot{\psi} & \phi & \dot{\phi} & Y & \psi\end{bmatrix}^{\mathrm{T}} \\ \boldsymbol{A} &= M^{-1}G \\ \boldsymbol{B} &= M^{-1}S \end{aligned}$$

with

$$M = \begin{bmatrix} mu_{\mathrm{s}x} & 0 & 0 & -m_{\mathrm{s}}h & 0 & 0 \\ 0 & I_{zz} & 0 & -I_{xz} & 0 & 0 \\ m_{\mathrm{s}}u_{\mathrm{s}x}h & I_{xz} & 0 & -I_{x\mathrm{eq}} & 0 & 0 \\ 0 & 0 & 1 & 0 & 0 & 0 \\ 0 & 0 & 0 & 0 & 1 & 0 \\ 0 & 0 & 0 & 0 & 0 & 1 \end{bmatrix}$$

$$\boldsymbol{G} = \begin{bmatrix} k_1 + k_2 & -mu_{\mathrm{s}x} + \frac{ak_1}{u_{\mathrm{s}x}} - \frac{bk_2}{u_{\mathrm{s}x}} & 0 & 0 & 0 & 0 \\ ak_1 - bk_2 & \frac{\left(a^2k_1 + b^2k_2\right)}{u_{\mathrm{s}x}} & 0 & 0 & 0 & 0 \\ 0 & -m_{\mathrm{s}}u_{\mathrm{s}x}h & k_{\mathrm{s}} - m_{\mathrm{s}}gh & c_{\mathrm{s}} & 0 & 0 \\ 0 & 0 & 0 & 1 & 0 & 0 \\ u_{\mathrm{s}x} & 0 & 0 & 0 & 0 & u_{\mathrm{s}x} \\ 0 & 1 & 0 & 0 & 0 & 0 \end{bmatrix}$$

$$\boldsymbol{S} = \begin{bmatrix} -k_1 & -k_1a & 0 & 0 & 0 & 0 \\ 0 & 1 & 0 & 0 & 0 & 0 \end{bmatrix}^{\mathrm{T}}$$

The lateral displacement and yaw angle are incorporated into the control strategy to lay the necessary foundation for position and yaw tracking of lane change for ACVs. The state equation of the control strategy is discretised so that the control strategy can run on the controller

$$x(k+1) = \boldsymbol{A}_{\mathrm{d}}x(k) + \boldsymbol{B}_{\mathrm{d}}u(k) \tag{37}$$

3.2.2 Enhanced state-space model considering trajectory preview: The real-time optimal trajectory of lateral lane change is real-time previewed and multiple previewed points are fed to the trajectory tracking controller. As shown in Fig. 6, the references of

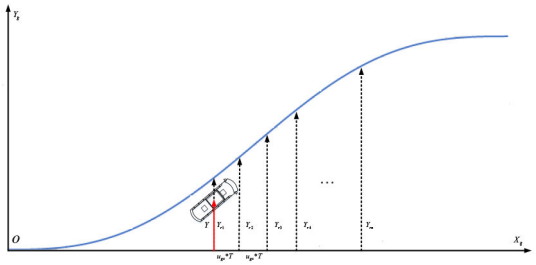

Fig. 6 *Multi-points preview of real time optimal trajectory for lateral lane change*

longitudinal and lateral displacements can be obtained by the multi-preview [24, 25, 34].

The transition relationship of longitudinal displacement is

$$X_{\mathrm{r}}(k+1) = X_{\mathrm{r}}(k) + u_{gx}T \tag{38}$$

The lateral displacements is the function of longitudinal displacement, as

$$Y_{\mathrm{r}}(k+1) = \frac{\mathrm{Re} * X_{\mathrm{r}}(k)}{\boldsymbol{D}} - \frac{\mathrm{Re}}{2\pi} * \sin\left(\frac{2\pi X_{\mathrm{r}}(k)}{\boldsymbol{D}}\right) \tag{39}$$

The state equation of lateral displacement is formed using the lateral displacement of multiple previewed points

$$Y_{\mathrm{r}}(k+1) = \boldsymbol{D}Y_{\mathrm{r}}(k) + \boldsymbol{E}Y_{rn}(k) \tag{40}$$

where

$$\boldsymbol{D} = \begin{bmatrix} 0 & 1 & 0 & \cdots & 0 \\ 0 & 0 & 1 & \cdots & 0 \\ \vdots & & & & \vdots \\ 0 & 0 & 0 & \cdots & 1 \\ 0 & 0 & 0 & \cdots & 0 \end{bmatrix} \quad \boldsymbol{E} = \begin{bmatrix} 0 \\ 0 \\ \vdots \\ 0 \\ 1 \end{bmatrix}$$

$$Y_{\mathrm{r}}(k) = [Y_{\mathrm{r1}}, Y_{\mathrm{r2}}], \ldots, Y_{rn}]^{\mathrm{T}}$$

The enhanced state-space model is realised combining the state equation (36) with the feed-forward of trajectory, as

$$\begin{aligned} \underbrace{\begin{bmatrix} x_{\mathrm{d}}(k+1) \\ Y_{\mathrm{r}}(k+1) \end{bmatrix}}_{Z(k+1)} &= \underbrace{\begin{bmatrix} \boldsymbol{A}_{\mathrm{d}} & 0 \\ 0 & \boldsymbol{D} \end{bmatrix}}_{A_Z} \underbrace{\begin{bmatrix} x(k) \\ Y_{\mathrm{r}}(k) \end{bmatrix}}_{Z(k)} \\ &+ \underbrace{\begin{bmatrix} 0 \\ \boldsymbol{E} \end{bmatrix}}_{E_z} Y_{rn}(k) + \underbrace{\begin{bmatrix} \boldsymbol{B}_{\mathrm{d}} \\ 0 \end{bmatrix}}_{B_z} \underbrace{\begin{bmatrix} \delta_{\mathrm{f}}(k) \\ \Delta M \end{bmatrix}}_{U(k)} \end{aligned} \tag{41}$$

where $\boldsymbol{Z} = \begin{bmatrix} \beta & \dot{\psi} & \phi & \dot{\phi} & Y & \psi & Y_{\mathrm{r1}} & Y_{\mathrm{r2}} & \cdots & Y_{rn} \end{bmatrix}^{\mathrm{T}}$

The lateral displacement and yaw angle are the characterisation and determinant of the trajectory, and thus considered as two control references. In addition, the ACV lateral acceleration should be reduced as much as possible to improve vehicle stability and passenger comfort. The lateral acceleration of the ACV

$$a_y = \underbrace{c_1\boldsymbol{A}}_{\boldsymbol{C}}x + \underbrace{c_1\boldsymbol{B}}_{\boldsymbol{D}}\begin{bmatrix} \delta_{\mathrm{f}}(k) \\ \Delta M \end{bmatrix} \tag{42}$$

where

$$c_1 = \begin{bmatrix} u_{\mathrm{s}x} & 0 & 0 & -\dfrac{m_{\mathrm{s}}h}{m} & 0 & u_{\mathrm{s}x} \end{bmatrix}$$

The lateral acceleration is discretised as

$$a_y(k+1) = C_{\mathrm{d}}x(k) + D_{\mathrm{d}}\begin{bmatrix} \delta_{\mathrm{f}}(k) \\ \Delta M \end{bmatrix} \tag{43}$$

The error of lateral displacement

$$e_y = Y - Y_{\mathrm{r1}} \tag{44}$$

The error of yaw angle

$$e_\psi \simeq \psi - \psi_{\mathrm{d}} = \psi - \frac{Y_{\mathrm{r2}} - Y_{\mathrm{r1}}}{x_{\mathrm{r2}} - x_{\mathrm{r1}}} = \psi - \frac{Y_{\mathrm{r2}} - Y_{\mathrm{r1}}}{u_{gx} * T} \tag{45}$$

The output equation of enhanced state-space is composed of the aforementioned three variables, as

$$\underbrace{\begin{bmatrix} e_y(k) \\ e_\psi(k) \\ a_y(k) \end{bmatrix}}_{Y_Z(k)} = \underbrace{\begin{bmatrix} \boldsymbol{E}_{\mathrm{c}} \\ \boldsymbol{AC}_{\mathrm{d}} \end{bmatrix}}_{C_Z} \underbrace{\begin{bmatrix} x(k) \\ Y_{\mathrm{r}}(k) \end{bmatrix}}_{Z(k)} + \underbrace{\begin{bmatrix} 0 \\ \boldsymbol{D}_{\mathrm{d}} \end{bmatrix}}_{D_Z} \underbrace{\begin{bmatrix} \delta_{\mathrm{f}}(k) \\ \Delta M \end{bmatrix}}_{U(k)} \tag{46}$$

where

$$\boldsymbol{E}_{\mathrm{c}} = \begin{bmatrix} 0 & 0 & 0 & 0 & 1 & 0 & -1 & 0 & 0 & \cdots & 0 \\ 0 & 0 & 0 & 0 & 0 & 1 & \dfrac{1}{u_{gx} * T} & -\dfrac{1}{u_{gx} * T} & 0 & \cdots & 0 \end{bmatrix}$$

$$\boldsymbol{AC}_{\mathrm{d}} = \begin{bmatrix} C_{\mathrm{d}} & 0 & 0 & 0 & \cdots & 0 \end{bmatrix}$$

3.2.3 LPV model formulation and gain-scheduling controller design: A matrix polytope can be described as the convex hull of a finite number of matrices with the same dimensions [33], such as

$$Co\{W_i, i = 1, \ldots, j\} := \left\{ \sum_{i=1}^{j} \sigma_i W_i : \sigma_i \geq 0, \sum_{i=1}^{j} \sigma_i = 1 \right\} \tag{47}$$

An LPV state-space model is written in the following form

$$\begin{aligned} \dot{x}' &= \boldsymbol{A}'(\rho)x' + \boldsymbol{B}'(\rho)u' \\ y' &= \boldsymbol{C}'(\rho)x' + \boldsymbol{D}'(\rho)u' \end{aligned} \tag{48}$$

where $\boldsymbol{A}'(\rho)$, $\boldsymbol{B}'(\rho)$, $\boldsymbol{C}'(\rho)$ and $\boldsymbol{D}'(\rho)$ are matrices of state space and depend on the time-varying parameter ρ. ρ is in the region formed by polytope, as

$$\rho \in \Theta := Co\{h_1, h_2, \ldots, h_j\} \tag{49}$$

Then, the state-space matrices $\boldsymbol{A}'(\rho)$, $\boldsymbol{B}'(\rho)$, $\boldsymbol{C}'(\rho)$, $\boldsymbol{D}'(\rho)$ can be written as

$$\begin{aligned} &\begin{pmatrix} \boldsymbol{A}'(\rho) & \boldsymbol{B}'(\rho) \\ \boldsymbol{C}'(\rho) & \boldsymbol{D}'(\rho) \end{pmatrix} \\ &\in Co\left\{ \begin{pmatrix} \boldsymbol{A}_i' & \boldsymbol{B}_i' \\ \boldsymbol{C}_i' & \boldsymbol{D}_i' \end{pmatrix} = \begin{pmatrix} \boldsymbol{A}'(h_i) & \boldsymbol{B}'(h_i) \\ \boldsymbol{C}'(h_i) & \boldsymbol{D}'(h_i) \end{pmatrix}, i = 1, \ldots, j \right\} \end{aligned} \tag{50}$$

ACV velocities are usually time-varying in the lateral lane change process. For instance, if the braking system works to maintain vehicle stability under the emergency conditions, the ACV velocities will change during the lateral lane change. In this view, the LPV model, in which ACV velocity is considered as the time-varying variable, is used to design the control strategy.

From (41) and (46)), it can be seen that the longitudinal velocity $u_{\mathrm{s}x}$ and its reciprocal $1/u_{\mathrm{s}x}$ are time-varying in $[u_{\min}, u_{\max}]$ and $[1/u_{\max}, 1/u_{\min}]$ [31]. The convex tetrahedron is defined including all possible values of uncertain matrices, as follows:

$$\begin{aligned} h_1 &= [u_{\min}, 1/u_{\max}] \quad h_2 = [u_{\min}, 1/u_{\min}] \\ h_3 &= [u_{\max}, 1/u_{\max}] \quad h_4 = [u_{\max}, 1/u_{\min}] \end{aligned} \tag{51}$$

Defining the following intermediate variables

$$\bar{\rho}_1 = \frac{u_{\max} - u_{sx}}{u_{\max} - u_{\min}} \quad \bar{\rho}_2 = \frac{u_{sx} - u_{\min}}{u_{\max} - u_{\min}}$$
$$\breve{\rho}_1 = \frac{1/u_{\min} - 1/u_{sx}}{1/u_{\min} - 1/u_{ax}} \quad \breve{\rho}_2 = \frac{1/u_{sx} - 1/u_{\max}}{1/u_{\min} - 1/u_{\max}} \tag{52}$$

the enhanced state-space model shown in (41) and (46) can be written as

$$Z(k+1) = \left[\sum_{i=1}^{4} \sigma_i A_z(h_i)\right] Z(k) + \left[\sum_{i=1}^{4} \sigma_i B_z(h_i)\right] U(k) + E_z Y_{(r+1)}(k) \tag{53}$$

and

$$Y_z(k) = \left[\sum_{i=1}^{4} \sigma_i C_z(h_i)\right] Z(k) + \left[\sum_{i=1}^{4} \sigma_i D_z(h_i)\right] U(k) \tag{54}$$

where $\sigma_1 = \bar{\rho}_1\breve{\rho}_1$, $\sigma_2 = \bar{\rho}_1\breve{\rho}_2$, $\sigma_3 = \bar{\rho}_2\breve{\rho}_1$, $\sigma_4 = \bar{\rho}_2\breve{\rho}_2$

The LQR algorithm, considered as the classical optimal algorithm, is used to calculate the controller gains. The objective function of trajectory tracking control is defined as

$$J = \sum_{k=0}^{\infty} \left\{ Q(Y_z(k))^2 + R(U(k))^2 \right\} \tag{55}$$

where

$$\boldsymbol{Q} = \begin{bmatrix} q_1 & 0 & 0 \\ 0 & q_2 & 0 \\ 0 & 0 & q_3 \end{bmatrix}, \quad \boldsymbol{R} = \begin{bmatrix} r_1 & 0 \\ 0 & r_2 \end{bmatrix}$$

are the weight coefficients of the controller.

The calculation of the control gains of the four vertexes $K(h_i)$ can be achieved by solving the Riccati (details can be found in [35]). Then, the gain-scheduling controller is obtained using

$$U(k) = -\sum_{i=1}^{4} \sigma_i K(h_i) * Z(k) \tag{56}$$

4 Simulations and hardware-in-loop test

To verify the proposed control strategy, three test conditions are designed

(i) Constant velocity of SVs.

(ii) Obstacle avoidance with time-varied acceleration and velocity of SVs.

(iii) Emergency condition with time-varied acceleration and velocity of SVs.

The performance of the control strategy can be fully demonstrated in the three conditions. The first two conditions are validated on the software simulation platform combining Matlab/Simulink and Trucksim, whereas the last condition is tested on HIL test bench based on PXI-1042 and built by the Simulink-Trucksim- real-time system interfaced using Labview. The software simulation platform using Trucksim and Matlab/Simulink is constructed as follows: the parameters of ACVs are set and the traffic environment is constructed by Trucksim. The acceleration and velocity of SVs are controlled, and the dynamic trajectory planning and tracking are constructed by the Matlab/Simulink. The information of ACVs states is real-time delivered to Matlab/Simulink. Based on the information, the steering angle or brake pressure is determined by running the proposed control strategy in the Matlab/Simulink. The determined control values are delivered to Trucksim, and are used to control the ACVs in the Trucksim. The overview of the HIL test bench is shown in Fig. 7.

The key parameters of the ACV are shown in Table 1.

Note that, in each scenario, once the ACV completes the lane change, the ACV is controlled to follow the centre line of the target lane and the length of trajectory no longer changes.

4.1 Simulations and analysis

4.1.1 Condition 1: constant velocity of SVs: The simulation condition is set as follows: the initial velocity of the ACV equals to 90 km h^{-1}, the initial velocities, longitudinal accelerations and distances of the front and the rear vehicles on the original lane and the front and the rear vehicles on the target lane are 36 km h^{-1}, 0 m s^{-2}, 70 m; 156 km h^{-1}, 0 m s^{-2}, 60 m and 72 km h^{-1}, 0 m s^{-2}, 70 m; 155 km h^{-1}, 0 m s^{-2}, 60 m; respectively. The performance of the proposed control strategy in normal lateral lane change can be illustrated in this case.

The simulation results are shown in Figs. 8 and 9. As shown in Fig. 8*a*, by carrying on the trajectory optimisation in the whole lateral lane change process, the longitudinal limits are determined. Within the longitudinal limits, the optimal longitudinal length can be acquired by minimising the objective function defined in (30). The trajectory of the ACV can be planned using the obtained optimal longitudinal length according to (6).

As shown in Figs. 8*c* and *d*, the ACV tracks well the trajectory reference generated in the trajectory planning phase. The maximum lateral displacement error of trajectory tracking is 0.05 m, accounting only for 1.5% of lateral distance.

The handing angle (Ψ) tracking is also an important aspect for a lateral lane change. According to Figs. 9*a* and *b*, the handing angle of the dynamic reference trajectory can be tracked well by the proposed control strategy. The maximum error of handing angle is the 0.07° and the maximum error percentage is 3.4% by

Fig. 7 *Overview of the HIL test bench*

Table 1 Parameters of the ACV

Parameter	m, kg	I, kg m^2	a, m	b, m	k_1, N/rad	k_2, N/rad
value	7388	38,170	2.995	1.495	208,860	513,650

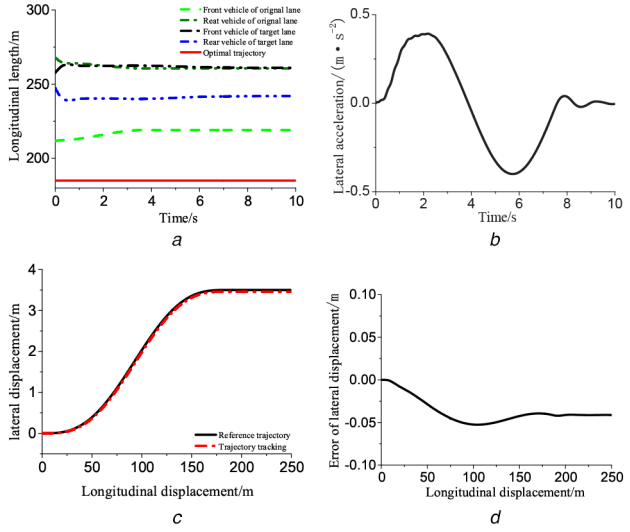

Fig. 8 *Simulation results in condition 1*

(a) Trajectory length, ***(b)*** Lateral acceleration, ***(c)*** Displacement tracking, ***(d)*** Error of displacement

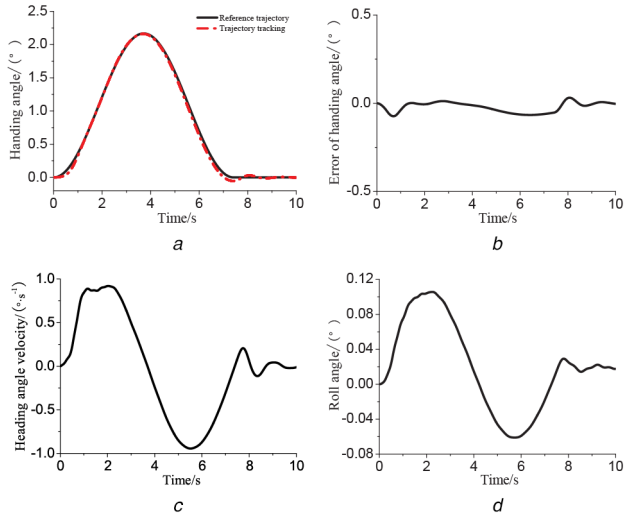

Fig. 9 *Simulation results in condition 1*

(a) Handing angle tracking, ***(b)*** Error of handing angle, ***(c)*** Heading angle velocity, ***(d)*** Roll angle

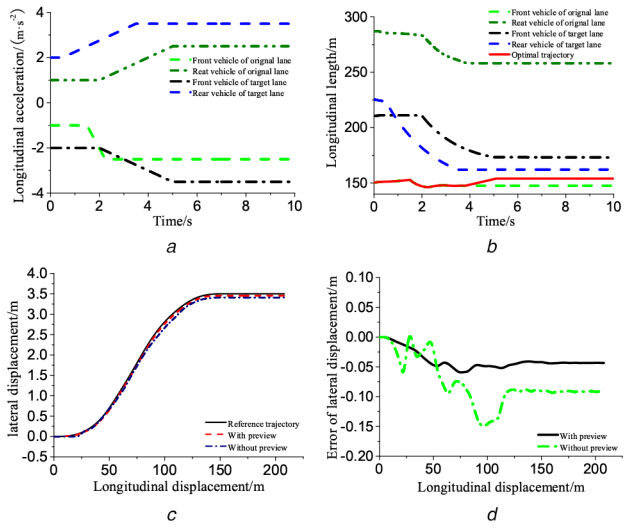

Fig. 10 *Simulation results in condition 2*

(a) Longitudinal acceleration, ***(b)*** Trajectory length, ***(c)*** Displacement tracking, ***(d)*** Error of displacement

calculation. So, the attitude of the ACV can change as the reference trajectory changes. Meanwhile, the good effect of the handing angle tracking can also improve the passenger comfort of lateral lane change for ACVs.

In Figs. 9*c* and *d* the handing angle velocity changes smoothly and the amplitude is small. Yaw stability can, therefore, be guaranteed. From Fig. 8*b*, the lateral acceleration is in the range of $\pm 0.5\ \mathrm{m\,s^{-2}}$ and changes smoothly during the whole process of the lateral lane change.

4.1.2 Condition 2: obstacle avoidance with a real-time change of acceleration and velocity of SVs: This situation is designed to verify the proposed control strategy in the situation that the ACV first avoids obstacle and then continues the lane change in the dynamic traffic environment.

The acceleration and velocity of the ACV and the SVs are set as follows: initial velocity of the ACV equal to $75\ \mathrm{km\,h^{-1}}$, the initial velocities and distances of the front and the rear vehicles on the original lane, and the front and the rear vehicles on the target lane are $52\ \mathrm{km\,h^{-1}}$, 35 m; $108\ \mathrm{km\,h^{-1}}$, 50 m and $65\ \mathrm{km\,h^{-1}}$, 20 m; $55\ \mathrm{km\,h^{-1}}$, 150 m; respectively. The real-time changing accelerations of the SVs are shown in Fig. 10*a*.

The longitudinal limits determined by four SVs are shown in Fig. 10*b*. The real-time optimal longitudinal length of planning trajectory for lateral lane change can be divided into two parts. The front part is before the separation point of the green line and red line; the rear part is after the separation point. In the front part, the optimal longitudinal length follows the limit of the front vehicle on the original lane. This process continues until the separation point. After that, the ACV will not collide with the vehicles on the original lane. Only the limits introduced by the vehicles on the target lane will be considered in trajectory planning.

As shown in Figs. 10*c* and *d*, the real-time reference trajectory can be well tracked smoothly by the proposed control strategy with small displacement error. The maximum lateral displacement error of trajectory tracking is 0.06 m and the maximum error percentage is 1.7%. According to the comparative calculation of the time when the reference trajectory and controlled trajectory reach to the maximum values, the delay time is about 30 ms.

In Figs. 11*a* and *b*, the proposed control strategy can adjust quickly to track well the reference of handing angle and the error is close to zero. Therefore, the obstacle avoidance performance during the lane change is verified. In Figs. 11*c* and 11*d*, the heading angle velocity and the sideslip angle are within the range of $\pm 2.3^{\circ}\,\mathrm{s^{-1}}$ and ±0.7°, respectively. Therefore, the yaw and roll stability of vehicle and passenger comfort can be maintained under the condition.

Meanwhile, to demonstrate the advantages of the proposed control strategy, the performance comparisons of different control strategies with multipoint preview and without preview are conducted in this condition. As shown in Figs. 10*c*, *d*, 11*a* and *b*, the performance comparisons indicate whether the tracking is a displacement tracking or a heading angle tracking, and it also indicates that the tracking performance with preview is better than that without preview.

4.2 Verification on the HIL test bench

Considering the high experiment cost, the influence of natural conditions and the large testing area of real vehicle test, a HIL test bench was constructed to simulate the fourth test condition in a quasi-real test environment.

On the HIL test bench, the emergency condition with real-time changing accelerations and velocities of SVs is simulated. The condition is set as follows: initial velocity of the ACV is equal to $80\ \mathrm{km\,h^{-1}}$, the initial velocities and distances of the front and the rear vehicles on the original lane and the front and the rear vehicles on the target lane are $18\ \mathrm{km\,h^{-1}}$, 20 m; $85\ \mathrm{km\,h^{-1}}$, 30 m; $85\ \mathrm{km\,h^{-1}}$, 24 m and $57\ \mathrm{km\,h^{-1}}$, 30 m; respectively. The real-time changing accelerations of SVs are shown in Fig. 12*a*. The condition is called an emergency due to the small space of lateral lane change caused by SVs.

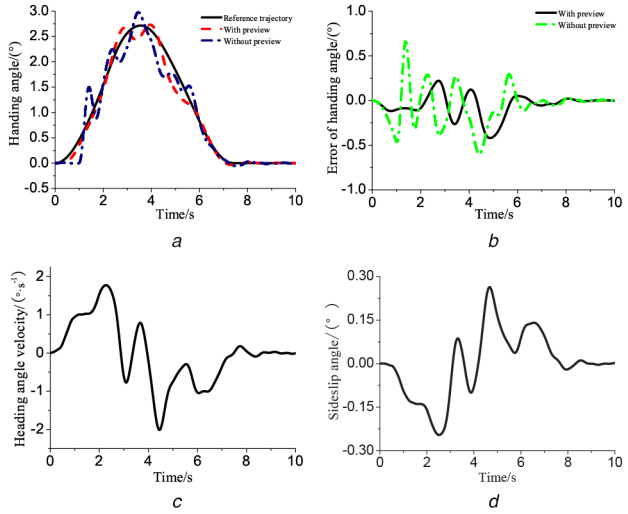

Fig. 11 *Simulation results in condition 2*

(a) Handing angle tracking, ***(b)*** Error of handing angle, ***(c)*** Heading angle velocity, ***(d)*** Sideslip angle

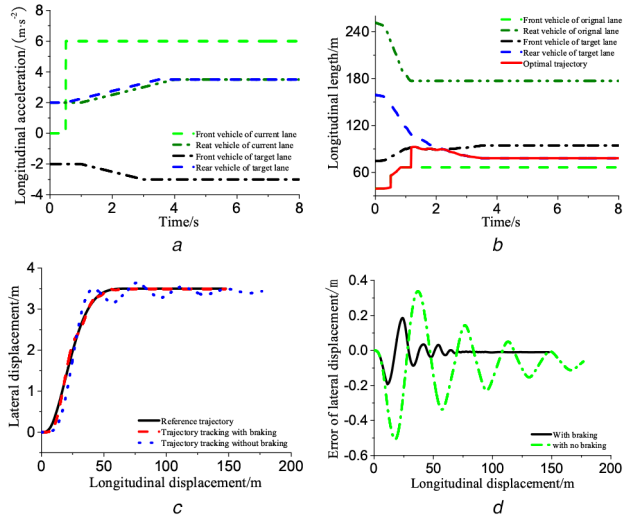

Fig. 12 *HIL experiment results in condition 3*

(a) Longitudinal acceleration, ***(b)*** Trajectory length, ***(c)*** Displacement tracking, ***(d)*** Error of displacement

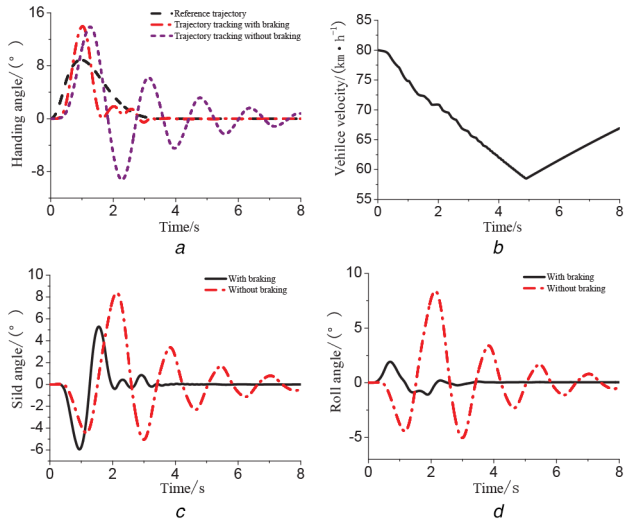

Fig. 13 *HIL experiment results in condition 3*

(a) Handing angle tracking, ***(b)*** Velocity, ***(c)*** Side angle, ***(d)*** Roll angle

As shown in Fig. 12*a*, the front vehicle on the original lane accelerates to expand distance when the ACV is too close to it. The longitudinal limits of the lane-changing trajectory determined by the four SVs are shown in Fig. 12*b*. The real-time optimal longitudinal length of planning trajectory is illustrated by the red curve. The curve can be divided into three parts. In the first part, the optimal trajectory length is obtained respecting the distance constraints carried by the vehicles of both the original lane and target lane. In the second and the third parts, the planned trajectory is constrained only by the positions of the vehicles in the target lane, as the safe distances from the ACV to the vehicles on the original lane can always be guaranteed. As shown in the figure, in the first part, the optimal planned trajectory follows the limit caused by the front vehicle in the original lane. The front and the rear vehicles in the target lane constrain the planned trajectory in the second and third parts, respectively.

To demonstrate the advantages of the proposed control strategy combining the steering system with braking system for an emergency condition, the control effect of the presented control strategy is compared with that of the control strategy with only the steering system. As shown in Figs. 12*c* and *d*, the trajectory reference can be well tracked using the proposed control strategy. Small displacement error is guaranteed. The maximum lateral displacement error is 0.17 m, accounting for the error percentage of 4.8%. Obviously, the control performance of the proposed control strategy is better than the control strategy only using the steering system.

According to Figs. 13*a* and *b*, the proposed control strategy can adjust quickly to track well the reference handing angle again and the error is close to zero. From Figs. 13*c* and *d*, the side angle and roll angle are within the stable range and the fluctuation is small. The proposed control strategy can cope with the emergency condition. However, the control performance with only steering system is not so satisfactory as the proposed one.

The target velocity of the ACV is set to 80 $\mathrm{km\,h^{-1}}$ at the beginning. In Fig. 13*b*, the velocity of the ACV decreases since there is a needful braking action in the lateral lane change. The velocity of the ACV increases to the target velocity when the braking action is disabled. Despite the velocity of the ACV changes dynamically, the proposed control strategy can also achieve good control of the lateral lane change. The proposed gain-scheduling control strategy based on enhanced LPV model is, therefore, verified to be able to adapt to the dynamic velocity of the ACV.

5 Conclusion

Control of lateral lane change is one of the key elements of ACV control. In this work, a DLLC control strategy based on real-time trajectory planning and LPV-based gain-scheduling trajectory tracking control is proposed. Different test conditions are designed to test the proposed strategy. From the results of software simulations and HIL experiments, it is concluded that

(i) The maximum longitudinal limits of lane change trajectory determined by the SVs on the original and target lanes are real time obtained according to the dynamic information like accelerations, positions and velocities of the ACV and the SVs.
(ii) By solving the constrained optimisation problem, optimal trajectory planning can be achieved in real-time and complex traffic environment caused by SVs.
(iii) Precise and stable trajectory tracking control can be realised thanks to a series of specific designs, including multi-step trajectory preview, the combination of steering control and braking control, LPV-based gain-scheduling control design.
(iv) The good performance of the proposed control strategy is verified in different traffic conditions, from constant velocity to varied velocity and acceleration of SVs and ACVs, from the normal DLLC condition to the emergency condition.

The ongoing work is oriented to verify the proposed control strategy in a real traffic environment.

6 Acknowledgments

This work was supported by the National Natural Science Foundation of China (Grant No. 51705225) and by the China Scholarship Council (Grant No. 201801810050).

7 References

[1] Cao, H., Song, X., Zhao, S., *et al.*: 'An optimal model-based trajectory following architecture synthesising the lateral adaptive preview strategy and longitudinal velocity planning for highly automated vehicle', *Veh. Syst. Dyn.*, 2017, **55**, (8), pp. 1143–1188

[2] He, X., Liu, Y., Lv, C., *et al.*: 'Emergency steering control of autonomous vehicle for collision avoidance and stabilisation', *Veh. Syst. Dyn.*, 2019, **57**, (8), pp. 1163–1187

[3] Vahidi, A., Sciarretta, A.: 'Energy saving potentials of connected and automated vehicles', *Transp. Res. C, Emerg. Technol.*, 2018, **95**, pp. 822–843

[4] Ji, X., He, X., Lv, C., *et al.*: 'Adaptive-neural-network-based robust lateral motion control for autonomous vehicle at driving limits', *Control Eng. Pract.*, 2018, **76**, pp. 41–53

[5] Jula, H., Kosmatopoulos, E.B., Ioannou, P.A.: 'Collision avoidance analysis for lane changing and merging', *IEEE Trans. Veh. Technol.*, 2000, **49**, (6), pp. 2295–2308

[6] Bevly, D., Cao, X., Gordon, M., *et al.*: 'Lane change and merge maneuvers for connected and automated vehicles: A survey', *IEEE Trans. Intell. Veh.*, 2016, **1**, (1), pp. 105–120

[7] Naranjo, J.E., Gonzalez, C., Garcia, R., *et al.*: 'Lane-change fuzzy control in autonomous vehicles for the overtaking maneuver', *IEEE Trans. Intell. Transp. Syst.*, 2008, **9**, (3), pp. 438–450

[8] You, F., Zhang, R., Lie, G., *et al.*: 'Trajectory planning and tracking control for autonomous lane change maneuver based on the cooperative vehicle infrastructure system', *Expert Syst. Appl.*, 2015, **42**, (14), pp. 5932–5946

[9] Gong, S., Du, L.: 'Cooperative platoon control for a mixed traffic flow including human drive vehicles and connected and autonomous vehicles', *Transp. Res. B, Methodol.*, 2018, **116**, pp. 25–61

[10] Hu, X., Sun, J.: 'Trajectory optimization of connected and autonomous vehicles at a multilane freeway merging area', *Transp. Res. C, Emerg. Technol.*, 2019, **101**, pp. 111–125

[11] Wang, Q., Ayalew, B., Weiskircher, T.: 'Predictive maneuver planning for an autonomous vehicle in public highway traffic', *IEEE Trans. Intell. Transp. Syst.*, 2018, **20**, (4), pp. 1303–1315

[12] Shim, T., Adireddy, G., Yuan, H.: 'Autonomous vehicle collision avoidance system using path planning and model-predictive-control-based active front steering and wheel torque control', *Proc. Inst. Mech. Eng., D, J. Automob. Eng.*, 2012, **226**, (6), pp. 767–778

[13] Kanaris, A., Kosmatopoulos, E.B., Loannou, P.A.: 'Strategies and spacing requirements for lane changing and merging in automated highway systems', *IEEE Trans. Veh. Technol.*, 2001, **50**, (6), pp. 1568–1581

[14] Anderson, S.J., Peters, S.C., Pilutti, T.E., *et al.*: 'Design and development of an optimal-control-based framework for trajectory planning, threat assessment, and semi-autonomous control of passenger vehicles in hazard avoidance scenarios'. Robotics Research, Lucerne, Switzerland, 2011, pp. 39–54

[15] Kayacan, E., Kayacan, E., Ramon, H., *et al.*: 'Towards agrobots: trajectory control of an autonomous tractor using type-2 fuzzy logic controllers', *IEEE/ASME Trans. Mechatronics*, 2014, **20**, (1), pp. 287–298

[16] Yang, D., Zheng, S., Wen, C., *et al.*: 'A dynamic lane-changing trajectory planning model for automated vehicles', *Transp. Res. C, Emerg. Technol.*, 2018, **95**, pp. 228–247

[17] Yang, D., Zhu, L., Liu, Y., *et al.*: 'A novel car-following control model combining machine learning and kinematics models for automated vehicles', *IEEE Trans. Intell. Transp. Syst.*, 2018, **20**, (6), pp. 1991–2000

[18] Luo, Y., Xiang, Y., Cao, K., *et al.*: 'A dynamic automated lane change maneuver based on vehicle-to-vehicle communication', *Transp. Res. C, Emerg. Technol.*, 2016, **62**, pp. 87–102

[19] Shah, J., Best, M., Benmimoun, A., *et al.*: 'Autonomous rear-end collision avoidance using an electric power steering system', *Proc. Inst. Mech. Eng., D, J. Automob. Eng.*, 2015, **229**, (12), pp. 1638–1655

[20] Yu, Z., Zhang, R., Xiong, L., *et al.*: 'Robust hierarchical controller with conditional integrator based on small gain theorem for reference trajectory tracking of autonomous vehicles', *Veh. Syst. Dyn.*, 2019, **57**, (8), pp. 1143–1162

[21] Li, X., Sun, Z., Cao, D., *et al.*: 'Development of a new integrated local trajectory planning and tracking control framework for autonomous ground vehicles', *Mech. Syst. Signal Process.*, 2017, **87**, pp. 118–137

[22] Outbib, R., Rachid, A.: 'Control of vehicle speed: a nonlinear approach'. Proc. of the 39th IEEE Conf. on Decision and Control, Sydney, Australia, 2000, vol. 1, pp. 462–463

[23] Abbassi, Y., Ait-Amirat, Y., Outbib, R.: 'Nonlinear feedback control and trajectory tracking of vehicle', *Int. J. Syst. Sci.*, 2015, **46**, (16), pp. 2873–2886

[24] Thommyppillai, M., Evangelou, S., Sharp, R.: 'Car driving at the limit by adaptive linear optimal preview control', *Veh. Syst. Dyn.*, 2009, **47**, (12), pp. 1535–1550

[25] Theunissen, J., Sorniotti, A., Gruber, P., *et al.*: 'Regionless explicit model predictive control of active suspension systems with preview', *IEEE Trans. Ind. Electron.*, 2020, **67**, pp. 4877–4888

[26] Guo, J., Li, K., Luo, Y.: 'Coordinated control of autonomous four wheel drive electric vehicles for platooning and trajectory tracking using a hierarchical architecture', *J. Dyn. Syst. Meas. Contr.*, 2015, **137**, (10), p. 101001

[27] Lian, Y., Wang, X., Tian, Y., *et al.*: 'Lateral collision avoidance robust control of electric vehicles combining a lane-changing model based on vehicle edge turning trajectory and a vehicle semi-uncertainty dynamic model', *Int. J. Automot. Technol.*, 2018, **19**, (2), pp. 331–343

[28] Hu, C., Jing, H., Wang, R., *et al.*: 'Robust h output-feedback control for path following of autonomous ground vehicles', *Mech. Syst. Signal Process.* ., 2016, **70**, pp. 414–427

[29] Erlien, S.M., Fujita, S., Gerdes, J.C.: 'Shared steering control using safe envelopes for obstacle avoidance and vehicle stability', *IEEE Trans. Intell. Transp. Syst.*, 2015, **17**, (2), pp. 441–451

[30] Gao, Y., Gordon, T., Lidberg, M.: 'Optimal control of brakes and steering for autonomous collision avoidance using modified Hamiltonian algorithm'. *Veh. Syst. Dyn.*, 2019, **57**, pp. 1224–1240

[31] Wang, R., Zhang, H., Wang, J.: 'Linear parameter-varying controller design for four-wheel independently actuated electric ground vehicles with active steering systems', *IEEE Trans. Control Syst. Technol.*, 2013, **22**, (4), pp. 1281–1296

[32] Liu, Y., Ji, X., Yang, K., *et al.*: 'Finite-time optimized robust control with adaptive state estimation algorithm for autonomous heavy vehicle', *Mech. Syst. Signal Process.*, 2020, **139**, p. 106616

[33] Guo, J., Luo, Y., Li, K.: 'Robust gain-scheduling automatic steering control of unmanned ground vehicles under velocity-varying motion', *Veh. Syst. Dyn.*, 2019, **57**, (4), pp. 595–616

[34] Cheng, C., Cebon, D.: 'Improving roll stability of articulated heavy vehicles using active semi-trailer steering', *Veh. Syst. Dyn.*, 2008, **46**, (S1), pp. 373–388

[35] Eugenio, A., Vicen, P., Joseba, Q., *et al.*: 'Gain-scheduling LPV control for autonomous vehicles including friction force estimation and compensation mechanism', *IET Control Theory Appl.*, 2018, **12**, (12), pp. 1683–1693